JBC RESEARCH ARTICLE

Antibacterial peptide CyclomarinA creates toxicity by deregulating the *Mycobacterium tuberculosis* ClpC1–ClpP1P2 protease

Received for publication, March 22, 2022, and in revised form, June 16, 2022 Published, Papers in Press, June 26, 2022,
https://doi.org/10.1016/j.jbc.2022.102202

Gabrielle Taylor[1], Yannick Frommherz[2,3], Panagiotis Katikaridis[2,3], Dominik Layer[4], Irmgard Sinning[4], Marta Carroni[5], Eilika Weber-Ban[1,*], and Axel Mogk[2,3,*]

From the [1]ETH Zurich, Institute of Molecular Biology and Biophysics, Zurich, Switzerland; [2]Center for Molecular Biology of the University of Heidelberg (ZMBH), DKFZ-ZMBH Alliance, Heidelberg, Germany; [3]Division of Chaperones and Proteases, Deutsches Krebsforschungszentrum (DKFZ), Heidelberg, Germany; [4]Heidelberg University Biochemistry Center (BZH), Heidelberg, Germany; [5]Swedish Cryo-EM Facility, Science for Life Laboratory Stockholm University, Solna, Sweden

Edited by Ursula Jakob

The ring-forming AAA+ hexamer ClpC1 associates with the peptidase ClpP1P2 to form a central ATP-driven protease in *Mycobacterium tuberculosis* (Mtb). ClpC1 is essential for Mtb viability and has been identified as the target of antibacterial peptides like CyclomarinA (CymA) that exhibit strong toxicity toward Mtb. The mechanistic actions of these drugs are poorly understood. Here, we dissected how ClpC1 activity is controlled and how this control is deregulated by CymA. We show that ClpC1 exists in diverse activity states correlating with its assembly. The basal activity of ClpC1 is low, as it predominantly exists in an inactive nonhexameric resting state. We show that CymA stimulates ClpC1 activity by promoting formation of supercomplexes composed of multiple ClpC1 hexameric rings, enhancing ClpC1–ClpP1P2 degradation activity toward various substrates. Both the ClpC1 resting state and the CymA-induced alternative assembly state rely on interactions between the ClpC1 coiled-coil middle domains (MDs). Accordingly, we found that mutation of the conserved aromatic F444 residue located at the MD tip blocks MD interactions and prevents assembly into higher order complexes, thereby leading to constitutive ClpC1 hexamer formation. We demonstrate that this assembly state exhibits the highest ATPase and proteolytic activities, yet its heterologous expression in *Escherichia coli* is toxic, indicating that the formation of such a state must be tightly controlled. Taken together, these findings define the basis of control of ClpC1 activity and show how ClpC1 overactivation by an antibacterial drug generates toxicity.

ATPase Associated with diverse cellular Activities (AAA+) proteases are central components of proteostasis networks in bacteria and play crucial roles for bacterial physiology and stress resistance by degrading not only aberrant proteins but also functional proteins harboring specific degrons for protease targeting (1, 2). AAA+ proteases are composed of a hexameric ring–forming ATPase (AAA+) component (*e.g.*, ClpA, ClpC), which associates with a barrel-forming peptidase (*e.g.*, ClpP). The proteolytic active sites are hidden in the interior of the peptidase barrel, protecting cellular proteins from unwanted degradation (3). Substrates access the degradation chamber *via* a continuous channel, which starts at the entry pore of the AAA+ hexamer. ATP hydrolysis by the AAA+ protein fuels the unfolding and threading of bound substrates into the peptidase barrel (4).

Protein degradation is irreversible and represents a potentially deleterious activity that has to be tightly controlled. Substrate selection and overall activity of AAA+ proteases are therefore precisely regulated. AAA+ proteins share the AAA domain, which is responsible for not only ATP binding and hydrolysis but also hexamerization. Substrate selectivity and activity control typically involve additional domains, which are either N-terminally fused to or inserted into the AAA module (N-terminal domain [NTD] and middle domain [MD], respectively). NTDs can directly recognize substrates, for instance, *Bacillus subtilis* (Bs) ClpC NTD recognizes phosphorylated arginine residues of substrates as degron (5). Alternatively, NTDs function as binding platforms for cooperating adaptor proteins that transfer their bound cargo to the AAA+ protein. The adaptor protein ClpS binds to N-end rule substrates, harboring destabilizing residues at their N termini and delivers them to the AAA+ partners ClpA or ClpC (6, 7). Adaptor proteins can in addition regulate the global activity of an AAA+ partner. Bs ClpC and *Staphylococcus aureus* (Sa) ClpC do not exhibit significant ATPase and proteolytic activities on their own but depend entirely on the presence of adaptors like MecA (8, 9). MecA triggers the formation of ClpC hexamers, a process that is linked to ATPase activation and the transfer of bound substrates (9, 10). MecA binds to both ClpC NTD and its coiled-coil MD (11). In the absence of MecA, MDs self-interact to form an alternative assembly state (resting state) that has very low ATPase activity and does not associate with ClpP (9). The resting state is formed by two

* For correspondence: Axel Mogk, a.mogk@zmbh.uni-heidelberg.de; Eilika Weber-Ban, eilika@mol.biol.ethz.ch.

pentameric half-spirals that are held together by head-to-head MD interactions. ClpC MD mutants that are deficient in MD self-interaction constitutively form hexamers and are toxic *in vivo* (9). This underlines the crucial role of MDs as negative regulators for ClpC activity control. The activation of ClpC by MecA is only temporary as the adaptor targets itself for degradation by ClpC–ClpP, ensuring ClpC inactivation once specifically targeted substrates have been degraded (8).

AAA+ proteases can play crucial roles in bacterial virulence (12). The AAA+ component ClpC1 of the important pathogen *Mycobacterium tuberculosis* (Mtb) is of particular interest as it forms an essential protease with the ClpP1P2 peptidase (13, 14). The crucial role of ClpC1–ClpP1P2 for Mtb viability qualifies the protease as an attractive drug target. Indeed, antibacterial compounds that target either ClpC1 or ClpP1P2 have been identified (15, 16). Acyldepsipeptide (ADEP) antibiotics target ClpP in multiple bacterial species triggering toxic ATPase-independent peptidase activation (17). In addition, ADEP competes with AAA+ components for binding to ClpP, thus in addition abrogating cooperation of ATPase and peptidase (18). ADEP antibiotics thereby exert dual effects on AAA+ proteases: the activation of ClpP enabling it for degradation of unstructured polypeptides and inhibition of ClpP cooperation with the AAA+ partner causing stabilization of folded substrates harboring specific degrons for protease targeting. ADEP toxicity in Mtb cells is based on the latter consequence (14). Diverse cyclic peptides, including lassomycin, ecumicin, rufomycin, and CyclomarinA (CymA), which are highly toxic to Mtb cells, target ClpC1 (19–22). All these compounds bind to a hydrophobic groove of ClpC1 NTD (23–25); however, their effects on ClpC1 ATPase and proteolytic activities seem diverse. Lassomycin and ecumicin increase ClpC1 ATPase activity (20, 21), whereas rufomycin shows no impact (22). All three peptides inhibit the degradation of the disordered model substrate casein by ClpC1–ClpP1P2, indicating peptide-induced uncoupling of ATPase and proteolytic activities (20–22). CymA activity has been characterized using a hybrid protein (N_{Mtb}–ClpC), composed of the Mtb ClpC1 NTD and the AAA and MD domains of Sa ClpC, which is insensitive to CymA in its WT form carrying the native NTD. For the hybrid fusion construct N_{Mtb}–ClpC, CymA increases both ATPase and proteolytic activities of the fusion construct (26). Whether CymA exerts the same enhancing effects on authentic Mtb ClpC1 or acts as an inhibitor like other cyclic peptides remained unknown. The understanding of drug mechanisms is hampered by a lack of knowledge about ClpC1 activity control. ClpC1 consists of two AAA domains (AAA1 and AAA2), an NTD, and a coiled-coil MD. While sharing the same domain organization with other bacterial ClpC proteins, it is unclear whether Mtb ClpC1 is regulated by a similar mechanism involving adaptor-controlled hexamer formation. Mtb ClpC1 exhibits autonomous proteolytic activity in contrast to Sa ClpC and Bs ClpC (20, 27, 28), indicating adaptor-independent hexamerization and differences in regulation. The stand-alone activity of ClpC1 is, however, low in comparison to MecA-activated Sa ClpC or Bs ClpC. This opens up the possibility that activation pathways also exist for ClpC1, suggesting in turn regulatory mechanisms are in place that downregulate its activity.

Here, we dissected ClpC1 activity control and its modulation by the drug CymA. We show that ClpC1 exists in different activity states caused by changes in assembly states. ClpC1 predominantly assembles into an inactive resting state, indicating that this regulatory mechanism is conserved among ClpC homologs. Abrogating the resting state by MD mutation leads to formation of ClpC1 hexamers that constitute the highest activity state of ClpC1. The drug CymA converts the resting state into a ClpC1 supercomplex built of multiple hexamers that interact with each other through their MDs. This assembly state shows increased proteolytic activities toward a diverse range of substrates tested, indicating that CymA toxicity toward Mtb cells is due to overactivation of the ClpC1–ClpP1P2 protease caused by resting state conversion to the hexamer supercomplex.

Results

Mtb ClpC1 forms an MD-dependent resting state

Sa ClpC activity is controlled by its coiled-coil MD that mediates the formation of an inactive resting state (9). Binding of the adaptor MecA to Sa ClpC NTD and MD prevents resting state formation and triggers formation of active ClpC hexamers. Mtb ClpC1 differs in various aspects from Sa ClpC. In a phylogenetic tree, Mtb ClpC1 localizes to a distinct branch, separating it from Sa ClpC (Fig. S1*A*). Notably, bacteria belonging to the Mtb ClpC1 clade do not encode for the canonical adaptor MecA, whereas MecA is present in all bacteria belonging to the Sa clade (Fig. S1*A*). This might suggest differences in the regulatory principles of both Hsp100 proteins. In agreement with this notion, Mtb ClpC1, in contrast to Sa ClpC, exhibits autonomous ATPase and proteolytic activities (20, 27, 28). However, ClpC1 ATPase and degradation activities are low as compared with MecA-activated Sa ClpC. Furthermore, ClpC1 also possesses the conserved phenylalanine (F444) at the tip of its MD, which was shown to be essential for resting state formation of Sa ClpC (Fig. 1*A*). These observations support the possibility that Mtb ClpC1 activity is also controlled by its MD. We therefore determined the oligomeric states of ClpC1 WT and the F444S mutant, probing for a potential role of the MD in controlling the assembly state (Fig. 1*B*). In size-exclusion chromatography (SEC) runs, ClpC1-WT eluted prior to the ClpC1-F444S mutant (Fig. 1*B*). The elution profiles of WT and F444S in the presence of nucleotide were very similar to those of Sa ClpC and *Escherichia coli* (Ec) ClpB serving as references for decameric resting and hexameric states, respectively. Mass determination of ClpC1-WT and ClpC1-F444S mutant complexes by multiangle light scattering measurements coupled to SEC runs (SEC–MALS) revealed that the diverse elution profiles are based on differences in molecular weight rather than shape (Fig. S1*B*). ClpC1-WT complexes had masses of 600 to 1160 kDa. Peak fractions had a molecular weight of 863 ± 81 kDa, corresponding to a nonameric complex, which is similar to the decameric resting state determined for Sa

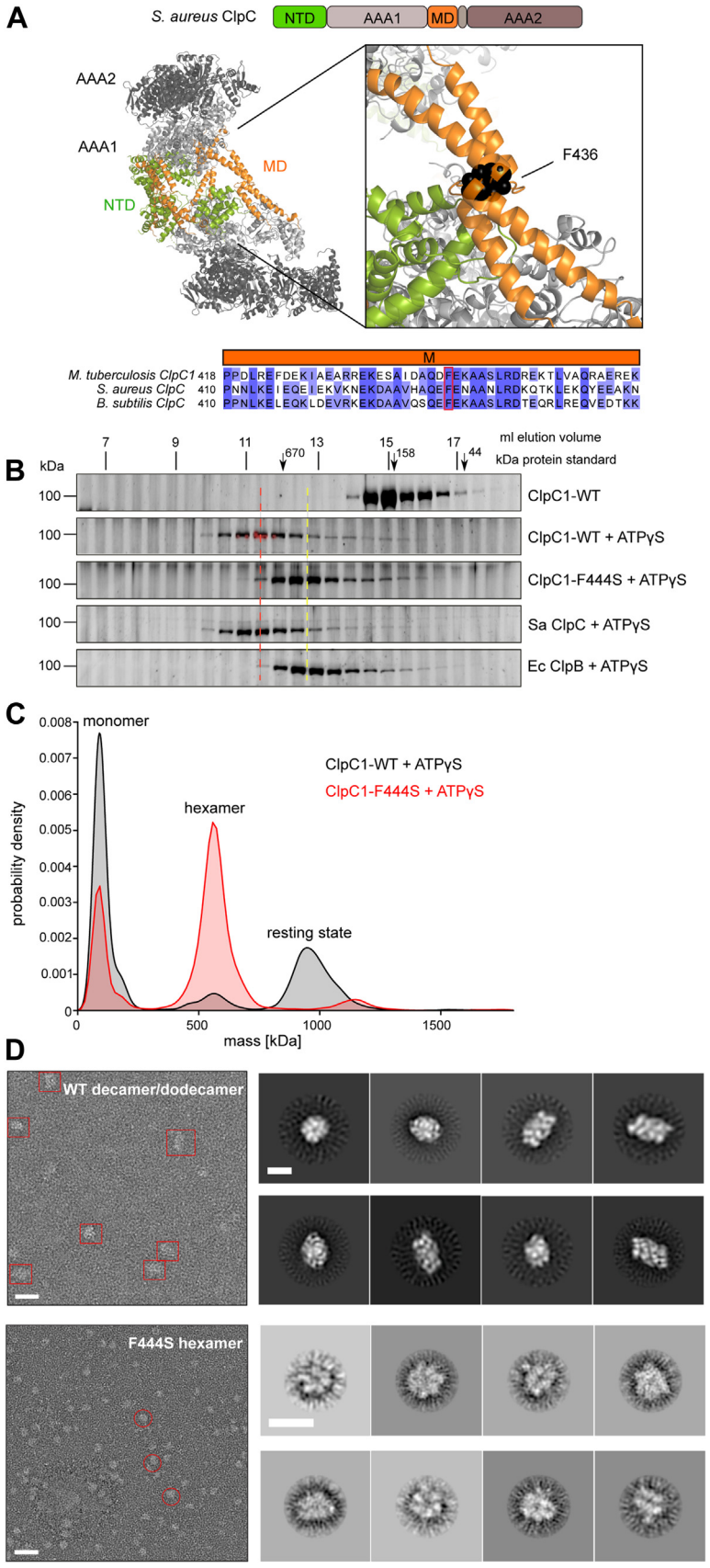

Figure 1. Mtb ClpC1 forms a resting state. *Top*, middle domain (MD)–mediated formation of the inactive resting state of *Staphylococcus aureus* (Sa) ClpC (Protein Data Bank entry: 6EM9) (9). The domain organization of Sa ClpC is provided. The conserved MD residue Phe436 located at the tip of the MD plays a crucial role in head-to-head interactions of MDs and resting state formation. *Bottom*, sequence alignment of the MD of the indicated ClpC proteins was generated using Clustal Omega (www.ebi.ac.uk/Tools/msa/clustalo/) and Jalview. The presence of a conserved tip-located phenylalanine residue (Mtb ClpC1

ClpC (9). ClpC1-F444S complexes had lower masses from 330 to 670 kDa and a molecular weight of 448 ± 58 kDa at the peak fraction corresponding to a pentameric complex. Such complex composition might result from partial dissociation of a ClpC1-F444S hexamer during the SEC–MALS run. To provide direct evidence for ClpC1-F444S hexamer formation, we performed glutaraldehyde crosslinking and analyzed the crosslink products by SDS-PAGE (Fig. S1*C*). In the presence of nucleotide, ClpC1-WT was mostly crosslinked to high molecular weight complexes that failed to enter the gel, whereas ClpC1-F444S predominantly formed crosslinked products that located at positions identical to crosslinked ClpB hexamers. Notably, ClpC1-WT crosslinking also yielded some hexameric products, which was not observed for Sa ClpC (Fig. S1*C*). This difference in crosslinking pattern correlates with the low autonomous activity described for Mtb ClpC1. We in addition employed mass photometry to determine molar masses of ClpC1 complexes in bulk solution avoiding complex disintegration during SEC runs. This technique allows to identify distinct protein complexes existing in a single preparation (Fig. 1*C*). At the low concentration of ClpC1 (60 nM) required for this methodology, both samples featured a mass peak of 86 to 91 kDa corresponding to a monomer was observed in the presence of slowly hydrolyzable ATPγS. ClpC1-WT in addition formed large complexes (mass range: 875–1260 kDa) with a mass of 968 ± 8 kDa at the most populated assembly state corresponding to a decameric (10.3-mer) resting state complex. Some smaller complexes (mass range: 450–700 kDa) with a mass of 563 ± 3 kDa at the peak were in addition present. This mass corresponds to a hexamer, which forms at much lower frequencies than the resting state (Fig. 1*C*). These data are consistent with crosslinking and former SEC results documenting the formation of high molecular weight complexes and the presence of some hexameric species. The formation of the larger complexes must involve the MD as the molar masses observed for ClpC1-F444S in the presence of nucleotide were much lower (480–620 kDa). The mass of the most populated ClpC1-F444S state was 563 ± 13 kDa, corresponding to a hexamer (Fig. 1*C*). We also noticed formation of larger complexes with ClpC1-F444S (1050–1250 kDa). Those had a different mass profile than ClpC1-WT complexes and were also much less populated. To directly visualize ClpC1-WT and ClpC1-F444S complexes, we performed negative-staining EM (Fig. 1*D*). EM analysis revealed the coexistence of diverse ClpC1-WT assemblies including hexamers and resting states, which constituted the most populated species. A low-resolution three-dimensional reconstruction (25 Å) of the resting state allowed rigid-body docking of up to 12 subunits, which were organized in two spiral subcomplexes that interacted *via* their MDs (Fig. S1*D*). ClpC1-F444S exclusively formed hexameric species (Fig. 1*D*). Together, our analysis of Mtb ClpC1 assembly states documents the formation of a resting state that is mediated by MD interactions.

CymA induces the formation of a ClpC1 supercomplex

CymA causes severe cellular toxicity in Mtb cells by binding to the ClpC1 NTD (19). We analyzed whether and how CymA binding modulates the ClpC1 assembly state. In crosslinking experiments, CymA hardly changed the crosslink patterns of ClpC1-WT or ClpC1-F444S (Fig. S1*C*). The intensity of the crosslinked band at the position of the hexamer remained the same for ClpC1-F444S, suggesting that it largely stayed hexameric. For ClpC1-WT, a slight decrease in the levels of ClpC1-WT hexamers was observed, but the main portion of ClpC1-WT was found in the band corresponding to higher molecular weight crosslinks (Fig. S1*C*). To better understand what constitutes the higher molecular weight fraction, SEC analysis was carried out. For this, we used the ATPase-deficient double Walker B variant ClpC1-E288A-E626A (DWB), which harbors mutations in the Walker B motifs of both AAA domains, to ensure highest complex stabilities (Fig. 2*A*). CymA binding caused a shift of ClpC1-DWB toward earlier elution fractions, implying the formation of larger complexes, which we confirmed by SEC–MALS analysis (Fig. S2*A*). CymA-induced ClpC1 complexes had a mass of 2500 to 3100 kDa; however, mass determination was not highly accurate as the concentration of eluting CymA-bound ClpC1-DWB remained low in multiple runs. CymA did not alter the elution profile of ClpC1-DWB-F444S in SEC runs (Fig. 2*A*), suggesting that CymA-induced changes observed for ClpC1-WT involve the MD. To overcome the limitations of the SEC–MALS runs, we determined the masses of CymA-induced ClpC1 assemblies by mass photometry in bulk solution (Fig. 2*B*). We observed large changes in mass distributions of ClpC1-WT complexes in the presence of CymA and ATPγS. The presence of CymA strongly reduced the fraction of ClpC1 masses representing the resting state while inducing the formation of larger complexes (2000–2500 kDa). The main peak of the mass distribution had a molecular weight of 2249 ± 111 kDa, corresponding to 24 ClpC1 subunits. No major changes in mass profiles were observed for ClpC1-F444S in the presence of CymA and ATPγS (Fig. 2*B*). This observation is consistent with SEC analysis (Fig. 2*A*) and confirms that CymA-induced changes in the ClpC1-WT assembly state involve the MD. To determine the nature of the 24-mer ClpC1–CymA complex, we applied EM; however, analysis suffered from poor image acquisition that could not be improved despite multiple attempts.

The formation of a CymA-induced ClpC1 complex consisting of 24 subunits is highly reminiscent of the

F444, Sa ClpC F436) is highlighted. *B*, oligomeric states of Mtb ClpC1-WT and ClpC1-F444S were determined in the presence of ATP by size-exclusion chromatography. Elution fractions were analyzed by SDS-PAGE. Elution profiles and peak positions of Sa ClpC and *Escherichia coli* (Ec) ClpB served as references for resting (*red dotted line*) and hexameric (*yellow dotted line*) states. Positions of peak fractions of a protein standard are indicated. Representative elution profiles out of three independent SEC runs are provided. *C*, mass distributions of Mtb ClpC1-WT (*black line*) and F444S (*red line*) were determined by mass photometry in the presence of 5 mM ATPγS. Representative mass profiles out of three independent experiments are shown. *D*, negative-stain comparison of ClpC1-WT and ClpC1-F444S complexes. *Left*, representative micrographs with examples of picked particles *boxed* or *circled*. *Right*, 2D class averages obtained for the WT and the F444S mutant. The scale bar represents 150 Å. Mtb, *Mycobacterium tuberculosis*.

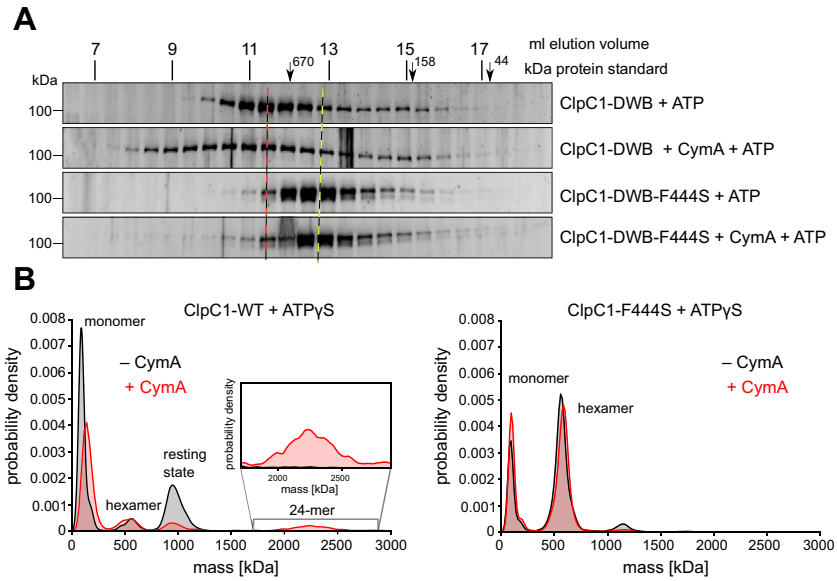

Figure 2. CymA induces the formation of large MD-dependent ClpC1 supercomplexes. *A*, oligomeric states of Mtb ClpC1-DWB and ClpC1-DWB-F444S were determined by size-exclusion chromatography (SEC) in the presence of ATP and CymA as indicated. Elution fractions were analyzed by SDS-PAGE. Positions of peak fractions of a protein standard are indicated. *Red and yellow dotted lines* indicate elution positions of ClpC1 resting state (*red*) and hexamers (*yellow*). Representative elution profiles out of three independent SEC runs are provided. *B*, mass distributions of ClpC1-WT and ClpC1-F444S assembled with 5 mM ATPγS in either the absence (*black line*) or the presence (*red line*) of CymA as determined by mass photometry. Representative mass profiles out of three independent experiments are shown. CymA, CyclomarinA; Mtb, *Mycobacterium tuberculosis*.

CymA-induced oligomerization changes observed for the N_{Mtb}–ClpC fusion construct (26). Here, EM analysis revealed a complex consisting of four hexamers that formed a triangular pyramid (26). As the effects of CymA on Mtb ClpC1 oligomerization involve the MD residue F444, we tested whether the same MD residue (F436) is also crucial for formation of 24-meric N_{Mtb}–ClpC complexes (Fig. S2*B*). Indeed, CymA presence did not alter the N_{Mtb}–ClpC-F436A elution profile in SEC runs, whereas it induced the formation of larger N_{Mtb}–ClpC complexes. We infer that CymA is causing similar changes in the assembly states of ClpC1 and N_{Mtb}–ClpC, converting the resting state into hexamers that can form higher assembly states in an MD-dependent manner.

CymA enhances Mtb ClpC1 ATPase activity and substrate binding

We determined the consequences of altered assembly states induced by either CymA or the F444S mutation on ClpC1 ATPase activity. CymA enhanced the basal ATPase activity of ClpC1 by 2.5-fold (Fig. 3*A*). This observation is similar to the stimulatory effect of CymA on N_{Mtb}–ClpC ATPase activity (26). Notably, we determined a strong synergistic effect of cooperating ClpP1P2 peptidase and the disordered model substrate casein on ClpC1 ATPase activity, resulting in a fourfold increase in the presence of both factors. CymA further enhanced ATP hydrolysis in the presence of casein and ClpP1P2 and led to the highest ATPase activity (Fig. 3*A*). ATPase activities of ClpC1-F444S, either alone or in the presence of ClpP1P2, casein, or CymA, were always higher as compared with ClpC1-WT (Fig. 3*A*). This links constitutive hexamer formation triggered by the F444S mutation to higher ATPase activities. Similarly, the stimulation of ClpC1 ATPase activity by CymA correlates with the conversion of the resting state into an assembly composed of hexamers. Titration of ATPase activity with increasing concentrations of CymA yielded a sigmoidal dose–response curve with a Hill coefficient of 3.2 ± 0.5. This suggests that binding of multiple CymA molecules to a ClpC1 hexamer is required for maximal ATPase stimulation (Fig. 3*B*). In order to analyze how CymA modulates substrate interaction, we determined binding affinities to fluorescently labeled casein (FITC-casein) using fluorescence anisotropy (Fig. 3*C*). Mtb ClpC1 bound only weakly to FITC-casein. The binding was strongly enhanced in the presence of CymA yielding a K_d of 1 μM. A similar binding affinity was determined for ClpC1-F444S in the absence and presence of CymA (Fig. 3*C*). These findings are consistent with a CymA-triggered conversion of the resting state into hexameric assemblies, which bind casein more efficiently. ClpC1-F444S adopts a hexameric state without CymA, explaining why its binding affinity to FITC-casein in the absence of CymA corresponded to the enhanced value observed with ClpC1-WT only in the presence of CymA and remained unaltered upon addition of CymA.

CymA enhances degradation of various ClpC1 substrates

We analyzed how CymA binding and the MD F444S mutation affects the proteolytic activity of ClpC1-WT–ClpP1P2. We first monitored the degradation of FITC-casein, which leads to an increase in fluorescence intensity because of fluorophore dequenching upon cleavage to short peptides (Fig. 4*A*). CymA increased the basal degradation activity of ClpC1-WT–ClpP1P2 by fourfold (Fig. 4*B*). ClpC1-F444S–ClpP1P2 exhibited threefold increased proteolytic activity as compared with ClpC1-WT–ClpP1P2, and FITC-casein

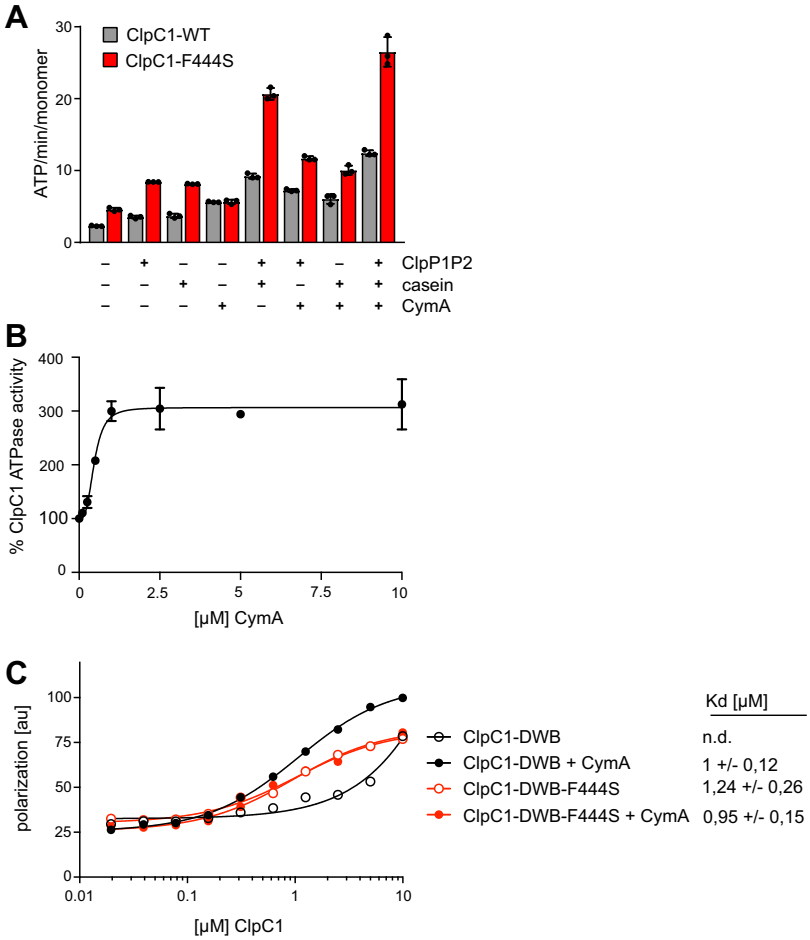

Figure 3. CymA enhances ClpC1 ATPase activity and substrate-binding capacity. *A*, ATPase activities of ClpC1-WT and ClpC1-F444S were determined in the presence of indicated components. *B*, ATPase activity of ClpC1 was determined in the presence of increasing CymA concentrations. *C*, binding of ClpC1-DWB and ClpC1-DWB-F444S to FITC-casein was monitored in the presence of ATP and CymA as indicated by determining changes in FITC-casein anisotropy. Calculated binding affinities are provided. CymA, CyclomarinA.

degradation was further enhanced in the presence of CymA reaching degradation rates similar to CymA-bound ClpC1-WT–ClpP1P2 (Fig. 4, *A* and *B*). These findings largely correlate with the structural states and ATPase activities we determined before and indicate that CymA binding and the F444S mutation increase overall ClpC1 activity. The finding that ClpC1-WT–ClpP1P2 exhibits autonomous degradation activity is in agreement with former findings (20, 27, 28) and is different from Sa ClpC–ClpP (9). We observed that Mtb ClpC1-WT can cooperate with Sa ClpP in substrate degradation, allowing us to directly compare both Hsp100 proteins and confirm the fundamental difference between them (Fig. S3, *A* and *B*). Mtb ClpC1-WT–Sa ClpP but not Sa ClpC–Sa ClpP complexes exhibited proteolytic activity toward FITC-casein. The impact of CymA and the F444S mutation on the proteolytic activity of ClpC1–Sa ClpP was comparable to those determined for ClpC1–ClpP1P2 complexes. Similarly, we observed synergistic stimulation of ClpC1-WT ATPase activity by casein and Sa ClpP, confirming that Sa ClpP can functionally replace Mtb ClpP1P2 (Fig. S3*C*).

We next studied whether CymA enhances the ATPase activity of a particular AAA domain. ClpC1 harbors two AAA domains (AAA1 and AAA2). We generated Walker B mutants that specifically inhibit ATP hydrolysis at either AAA1 (E288A, WB1) or AAA2 (E626A, WB2). CymA stimulated ATP hydrolysis of ClpC1-E288A but not ClpC1-E626A, indicating that ATP hydrolysis at AAA2 is primarily enhanced upon drug binding (Fig. S3, *D* and *E*). The AAA2 domain constitutes the main threading motor of Hsp100 proteins (29, 30), rationalizing the impact of CymA on ClpC1 activity. Notably, CymA did not enhance FITC-casein degradation by either of the ClpC1 Walker B mutants, indicating that ATPase stimulation of the AAA2 domain is not sufficient for increased proteolytic activity, which requires two functional ATPase rings (Fig. S3, *E* and *F*).

How general is the impact of CymA on ClpC1 proteolytic activity? To answer this question, we determined the effects of CymA and F444S on the degradation of a folded model substrate by monitoring degradation of GFP-SsrA, harboring the SsrA degron for Hsp100 targeting. CymA enhanced GFP-SsrA degradation of ClpC1-WT–ClpP1P2 by 1.8-fold. ClpC1-F444S–ClpP1P2 exhibited a 3.7-fold higher GFP-SsrA degradation rate compared with ClpC1–ClpP1P2, confirming its enhanced activity state. This activity was slightly reduced in

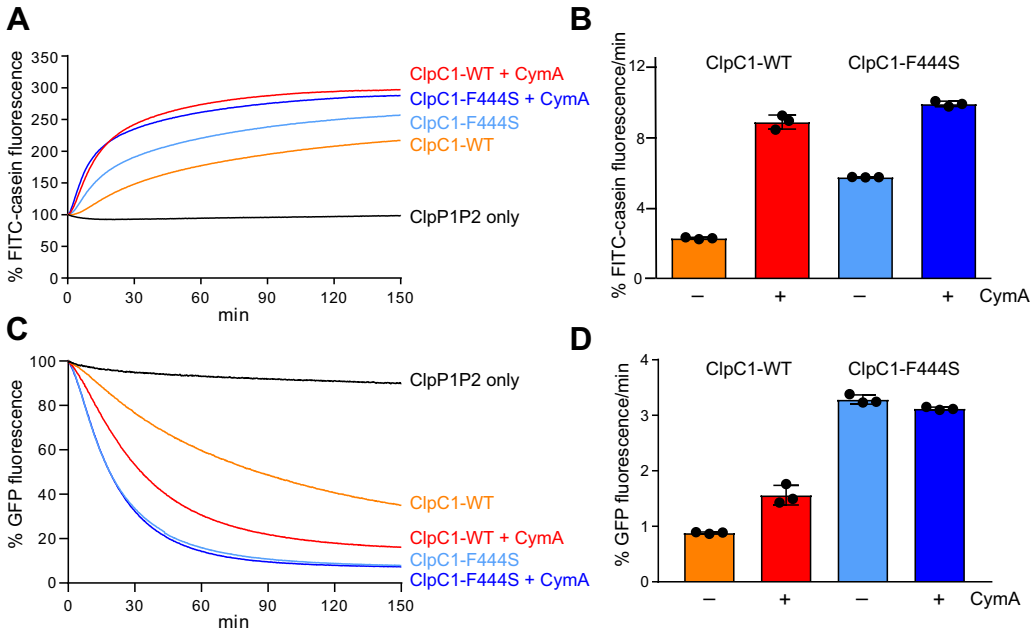

Figure 4. CymA increases proteolytic activity of ClpC1. *A*, FITC-casein degradation by ClpC1-WT and ClpC1-F444S was monitored in the presence of Mtb ClpP1P2 without or with CymA. Initial FITC-casein fluorescence was set to 100. FITC-casein degradation is linked to increase in fluorescence intensity, which is quenched in full-length casein. *B*, FITC-casein degradation rates were determined from the initial linear increase of FITC fluorescence. Initial FITC-casein fluorescence was set as 100, and relative changes in fluorescence were recorded. *C*, GFP-SsrA degradation was monitored by determining the loss of GFP fluorescence in the presence of ClpC1-WT or ClpC1-F444S and ClpP1P2 without or with CymA as indicated. *D*, GFP-SsrA degradation rates were determined from the initial linear decrease of GFP-SsrA fluorescence. CymA, CyclomarinA.

the presence of CymA (Fig. 4, *C* and *D*), in contrast to our findings for FITC-casein (Fig. 4, *A* and *B*), indicating substrate-specific effects of the drug. Notably, for ClpC1-F444S–ClpP1P2, we also observed an inhibitory effect of CymA on the degradation of the antitoxin VapB15, which represents a natural ClpC1 substrate (Fig. S4*A*) (7). CymA did not increase VapB15 degradation by ClpC1-WT–P1P2, and we rather observed a minor inhibition, again documenting substrate-specific effects (Fig. S4*A*).

We infer that CymA and the F444S mutation cause increased ClpC1 proteolytic activities toward multiple substrates, irrespective of their folding states or targeting signals. Although CymA does not affect degradation of all substrates equally, we did not observe strong inhibition of ClpC1-WT–ClpP1P2 activity as reported for other antibacterial peptides (20–22).

CymA and MD F444S mutation enhance ClpS-dependent substrate degradation

ClpS currently represents the only known adaptor protein of ClpC1. ClpS targets N-end rule substrates that harbor destabilizing residues (*e.g.*, Phe) at their N termini for degradation (6, 7, 31). We therefore studied how CymA and the F444S mutation affect degradation of the N-end rule model substrate FR-L-GFP (Fig. 5, *A* and *B*). CymA and F444S enhanced FR-L-GFP degradation rates by 1.6-fold and 8-fold, resembling their effects on GFP-SsrA. ClpS did not alter the basal ATP hydrolysis rates of ClpC1-WT and ClpC1-F444S in the absence or the presence of CymA (Fig. S4*B*). We also did not observe an impact of ClpS on ClpC1 crosslinking patterns (Fig. S4*C*), suggesting that ClpS solely acts as specificity factor without enhancing overall ClpC1 activity. Notably, CymA presence reduced the ClpS-dependent degradation activity of ClpC1-F444S by 2.3-fold (Fig. 5, *A* and *B*). Both CymA and ClpS

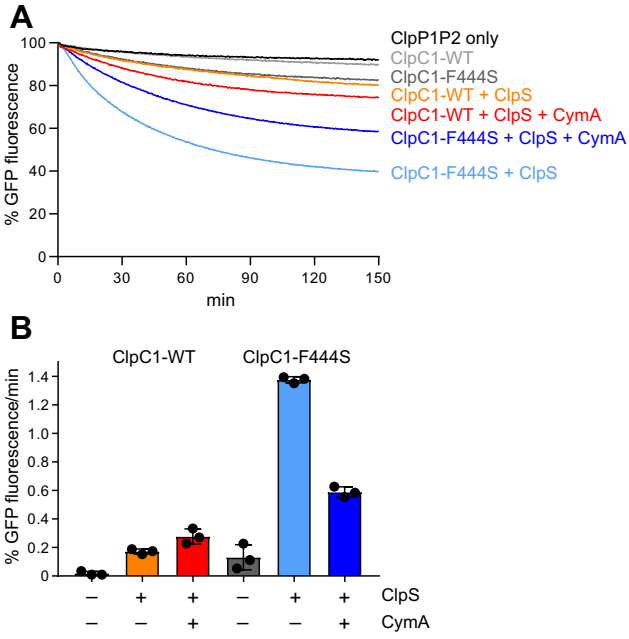

Figure 5. CymA modulates the ClpS-dependent degradation of an N-end rule model substrate. *A*, degradation of FR-L-GFP was monitored by determining the loss of GFP fluorescence in the presence of ClpC1-WT or ClpC1-F444S and ClpP1P2 without or with ClpS and CymA as indicated. *B*, FR-L-GFP degradation rates were determined from the initial linear decrease of GFP-SsrA fluorescence. CymA, CyclomarinA.

bind to ClpC1 NTD; however, their interaction sites do not overlap (Fig. S4*D*). This implies that CymA might alter the relative orientation of NTDs and bound ClpS, thereby hampering transfer of FR-L-GFP to the processing of ClpC1 pore site.

Loss of ClpC1 activity control by MD mutation increases cellular toxicity

We finally tested whether the modulations of ClpC1 activity states by the F444S mutation causes cellular toxicity. We made use of our finding that Mtb ClpC1 cooperates with Sa ClpP and coexpressed both genes from IPTG-controlled expression vectors in *Ec* host cells. This heterologous expression enabled us to directly determine the potentially toxic consequences of ClpC1 deregulation in the absence of so far unknown regulatory proteins that might control ClpC1 activity in *M. tuberculosis* cells. Co-overexpression of Mtb ClpC1 and Sa ClpP was toxic to *Ec* cells in a temperature-dependent manner and was observed at 37 °C (Figs. 6 and S5*A*). Coexpression of Sa *clpP* increased toxicity at least 100-fold, indicating that cells are killed by Mtb ClpC1–mediated protein degradation. This finding is consistent with the autonomous degradation activity of Mtb ClpC1–Sa ClpP determined *in vitro*. The presence of authentic *Ec* ClpP does likely not interfere with toxicity, as it does not cooperate with ClpC1-WT or ClpC1-F444S *in vitro* (Fig. S5*C*). Toxicity was increased approximately 10-fold upon expression of ClpC1-F444S (Fig. 6). Increased toxicity of ClpC1-F444S was also observed in the absence of Sa ClpP expression but not to the same extent as in its presence. Expression levels of ClpC1-WT and ClpC1-F444S were identical (Fig. S5*B*), indicating that the increased activity of ClpC1-F444S causes enhanced killing of *Ec* cells.

Discussion

In the present work, we show that regulation of Mtb ClpC1 activity crucially involves the MD-mediated formation of an inactive resting state. We validated the formation of this structural state by multiple techniques and by showing that mutating a conserved aromatic residue, which is obligatory for resting state formation by Sa ClpC, also triggers constitutive hexamer formation and activation of ClpC1. A recent study also documents resting state formation for Bs ClpC (32), indicating that ClpC activity control *via* MD-mediated resting state formation is widespread and evolutionarily conserved.

While sharing the basic regulatory mechanism with other bacterial ClpC homologs, Mtb ClpC1 also exhibits differences as it shows low autonomous proteolytic activity toward the disordered model substrate casein, which is not observed for Sa ClpC and Bs ClpC (9, 10). Similarly, coexpression of Mtb ClpC1 and cooperating Sa ClpP creates toxicity in *Ec* cells, which is not observed upon coexpression of Sa ClpC and Sa ClpP (9). We show here that this stand-alone ClpC1 activity is linked to adaptor-independent hexamer formation. We suggest that ClpC1 hexamers and the resting state exist in a dynamic equilibrium. This also implies that MD-mediated ClpC1 activity control is less stringent compared with other ClpC homologs and opens additional pathways for ClpC activation. We find that the simultaneous presence of substrate casein and a cooperating peptidase enhances ClpC1 ATPase activity, implying increased hexamer formation. ClpP1P2 forms a rigid double heptamer, which might serve as an assembly platform that facilitates ClpC1 hexamer formation or stabilizes ClpC hexamers upon interaction. The autonomous ClpC1-WT activity, however, remains low as evident from decreased proteolytic activities in comparison to ClpC1-F444S. This difference in proteolytic activity is particularly pronounced for tightly folded model substrates like GFP-SsrA and FR-L-GFP. The difference in ClpC1-WT and ClpC1-F444S activities remains in the presence of ClpS indicating that ClpS solely acts as specificity factor but does not increase overall ClpC activity as other adaptors like MecA. It is tempting to speculate that Mtb encodes for a ClpC1 adaptor that triggers an activity state comparable to ClpC1-F444S. This could be achieved by adaptor binding to the MDs or by covalently modifying ClpC1, ultimately abrogating resting state formation. However, such a putative activator would not be expected to be expressed constitutively, as persistent activation by MD mutation is toxic in case of Sa ClpC and Bs ClpC (9) and, similarly, we show increased toxicity of ClpC1-F444S as compared with ClpC1-WT upon heterologous expression in *Ec*. This predicts that an activation of Mtb ClpC1 will be tightly controlled and temporally limited.

ClpC1 represents the target of various cyclic peptides with strong antibacterial activities. Most of these compounds inhibit ClpC1–ClpP1P2 proteolytic activity toward FITC-casein

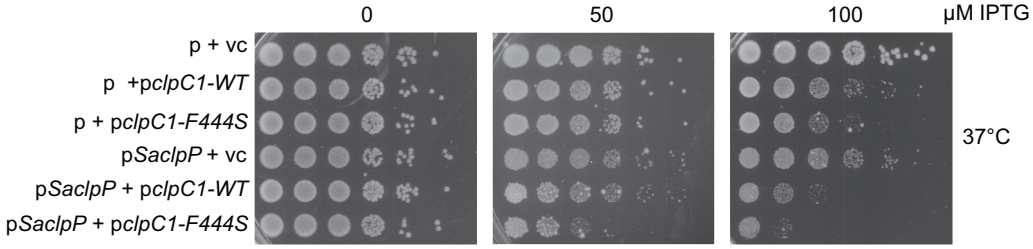

Figure 6. Overriding ClpC1 activity control creates toxicity. *Escherichia coli* XL1 cells harboring pUHE21- and pDMI.1-based plasmids for IPTG-controlled expression of *Staphylococcus aureus clpP* (p*SaclpP*) and indicated *clpC1* alleles (*clpC1-WT*, *clpC1-F444S*) and empty vector controls (p: pDMI.1; p*SaclpP*: pDMI.1-*Sac.lpP*; vc: pUHE21; *pclpC1-WT* (*F444S*): pUHE21-*clpC1-WT* [or *F444S*]) were grown overnight and adjusted to an absorbance of 1 at 600 nm. Serial dilutions (10^{-1}–10^{-6}) were spotted on LB plates containing the indicated IPTG concentrations and incubated at 37 °C for 24 h. Representative plates out of three independent experiments are provided.

in vitro, rationalizing toxicity toward Mtb cells. We show here that CymA acts differently, as it enhances ClpC1–ClpP1P2 degradation activity toward most substrates tested, including FITC-casein. A significant inhibition of proteolytic activity is not observed for ClpC1-WT. These findings are consistent with former results using the hybrid N_{Mtb}–ClpC fusion construct (26) indicating that CymA kills Mtb cells by inducing deregulated proteolysis. The effects of CymA on ClpC1–ClpP1P2 activity are in part substrate specific as an enhancement of VapB15 degradation was not observed. We envision a scenario in which CymA can have dual effects, negative and positive ones, on ClpC1 function. While CymA overrides MD-mediated ClpC1 activity control and enhances its ATPase activity, it might also hamper binding to substrates like VapB15. Our data on the constitutively hexameric population of ClpC1-F444S might serve as a model for a putative adaptor–activated state. For this variant, we observe a reduction in degradation activity toward the N-end rule model substrate. A scenario can thus be envisioned where under specific adaptor-activated conditions, CymA may inhibit degradation of specific substrates, like for example, N-end rule substrates. In the sum, these opposing effects level out, explaining the largely unchanged degradation of VapB15 by ClpC1-WT–ClpP1P2 in the presence of CymA.

It remains unknown why CymA can increase ClpC1 activity in contrast to other cyclic peptides. All peptides bind to the same groove of the NTD, yet the binding modes can be different as for instance, two ecumicin peptides bind to the NTD (25) (Fig. S6*A*). It is conceivable that diverse binding modes of CymA and ecumicin have different consequences on ClpC1 activity. However, rufomycin and CymA bind in an almost identical manner to ClpC1 NTD (Fig. S6*B*), leaving the question why both peptides have opposing effects on ClpC1 activity unanswered.

The stimulatory effect of CymA is based on its effect on the ClpC1 resting state, which is converted to an alternative assembly state built from hexamers. Mass determination of CymA-bound ClpC1 in an all-ATP state suggests a supercomplex composed of four hexamers, which is identical to the N_{Mtb}–ClpC assembly state triggered upon CymA binding (26). Notably, an analogous arrangement of ClpC hexamers has been recently reported for Bs ClpC bound to a substrate that harbors a phosphoarginine (pArg) group as targeting degron (32). Here, four ClpC hexamers form a tetrahedron, which is highly similar to the architecture of CymA-bound N_{Mtb}–ClpC (26). Remarkably, the four pArg-bound ClpC hexamers are held together *via* head-to-head MD interactions involving the MD tips (32). We show here that mutating F444 (or F436) located at the MD tip of Mtb ClpC1 (or N_{Mtb}–ClpC) prevents the formation of CymA-induced supercomplexes, providing further evidence that the organizations of CymA and pArg-induced ClpC assemblies are largely similar (Fig. 7). In this ClpC1 supercomplex, the AAA2 ring is fully accessible for ClpP1P2 interaction, explaining why the increase in ClpC1 ATPase activity in the presence of CymA is linked to enhanced proteolytic activity. How the binding of CymA to ClpC1 NTDs, which are not directly involved in resting state formation, converts the resting state into the tetrahedral supercomplex remains to be explored. As CymA does not bind to

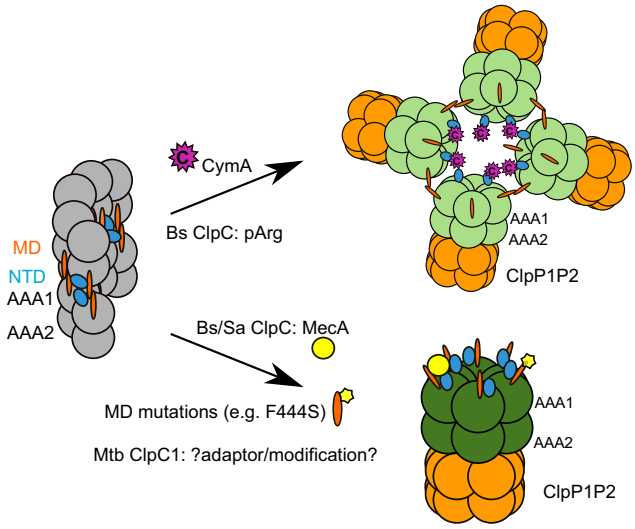

Figure 7. ClpC1 activity is determined by diverse assembly states. Mtb ClpC1 predominantly assembles into an inactive resting state, which has low ATPase activity and cannot associate with ClpP1P2. CymA binding abrogates resting state formation and triggers the formation of a ClpC1 superassembly that consists of four hexamers. This state exhibits intermediate activity and associates with ClpP1P2 *via* AAA2 domains. In *Bacillus subtilis* (Bs) ClpC, such state is induced upon binding of substrates harboring phosphorylated arginines as degron. A ClpC1 MD mutant (F444S) constitutively forms a highly active hexamer, a state that is triggered in Bs and *Staphylococcus aureus* (Sa) ClpC upon binding of the MecA adaptor protein. Mtb ClpC1 hexamerization might be triggered by modification or binding of so far unidentified adaptors. MD, middle domain; Mtb, *Mycobacterium tuberculosis*.

regulatory MDs, those are still free for self-interaction, now mediating the interaction of individual hexamers. The finding that CymA acts on the ClpC1 resting state implies that drug-based overactivation can also be applied as antibacterial strategy for other major pathogens (*e.g., S. aureus*) harboring ClpC homologs that are regulated *via* the same mechanism.

The activity of CymA-activated ClpC1 is typically lower as compared with ClpC1-F444S, which only forms single hexamers as the mutated MDs can no longer interact. This observation indicates that ClpC can adopt diverse activity states depending on the assembly formed (Fig. 7). The factors triggering the individual structural and activity states are diverse and include not only specific adaptors (*e.g.*, MecA) but also degrons (*e.g.*, pArg) leading to full or partial ClpC activation, respectively. This way ClpC activities can be fine-tuned and adjusted to the particular cellular target. CymA interference can occur at multiple levels, including redistribution of the relative population of the various ClpC1 assembly states. The induction of active ClpC assemblies is typically transient as both substrates and activating adaptors are subjected to ClpC-dependent degradation, automatically limiting ClpC activation. In contrast, ClpC1 activation by CymA is constitutive. CymA thereby utilizes existing ClpC activation pathways while circumventing their built-in deactivation routines.

Experimental procedures

Strains, plasmids, and proteins

Ec strains used were derivatives of XL1-blue or BL21. Mtb ClpC1 was amplified by PCR, inserted into pET24a or pUHE21

expression vectors, and verified by sequencing. ClpC1-F444S was generated by PCR-based mutagenesis and verified by sequencing.

Mtb ClpC1 was purified after overproduction from Ec BL21 cells using nickel–iminodiacetic acid (Macherey–Nagel) following standard protocols. Eluted samples containing ClpC1 were pooled and further purified by SEC (Superdex S200; GE Healthcare) in 50 mM Hepes (pH 7.5), 150 mM KCl, 20 mM $MgCl_2$, 2 mM DTT, and 5% (v/v) glycerol. Mtb ClpP1P2, ClpS, and Sa ClpP were purified as described before (7, 9). Protein concentrations refer to monomers and were determined with the Bio-Rad Bradford assay using bovine serum albumin as standard.

SEC and SEC–MALS

Oligomeric states of Mtb ClpC1, Sa ClpC, or Ec ClpB (each 6 μM) were monitored by SEC (Superose 6 HR10-30; GE Healthcare) in buffer A (50 mM Tris [pH 7.5], 25 mM KCl, 20 mM $MgCl_2$, 2 mM DTT, and 10% [v/v] glycerol) supplemented with 2 mM ATP at 4 °C. Samples were preincubated with 2 mM ATPγS or 2 mM ATP (ClpC1-DWB) for 5 min prior injection. CycA (12 μM) was added as indicated. Fractions were collected in 96-well plates, aliquots taken, and subjected to SDS-PAGE. Gels were stained using SYPRO Ruby Protein Gel Stain (Thermo Fisher Scientific) following the manufacturer's instructions.

SEC–MALS experiments were performed using 6 μM ClpC1 and 12 μM CymA at room temperature using a Superose 6 HR10-30 column. The column was connected to a MALS system (Dawn Heleos II 8+ and Optilab T-rEX; Wyatt Technology). Data were analyzed using the Astra 6 software (Wyatt Technology).

Mass photometry

Mass photometry was used to compare the oligomeric state of ClpC1-WT and ClpC1-F444S in either the presence or the absence of CymA. About 0.5 μM ClpC1 was prepared in buffer B (50 mM Hepes [pH 7.5], 25 mM KCl, 5 mM ATPγS, 20 mM $MgCl_2$, 1 mM DTT, and 5% [v/v] glycerol) with 10 μM CymA added as indicated. To find focus, 15 μl buffer B was loaded within CultureWell gaskets (Merck on high-precision coverslips (ThorLabs). After finding focus, 2 μl ClpC1 was added to the buffer, and 60 s movies of landing events were recorded on the Refeyn One^{MP} mass photometer instrument using a frame rate of 100 Hz. The interferometric scattering contrast values of landing events were used to determine molecular mass values in the Discover^{MP} software following calibration with NativeMark unstained protein standard (Thermo Fisher Scientific). More than 2000 particles were detected in each movie (typically 3000–5000 landing events). Kernal density estimates were computed in the Python KDEpy 1.1.0 package (https://github.com/tommyod/KDEpy) using the FFTKDE function with a Gaussian kernel and a bandwidth of 20. Mass values were determined in the Discover^{MP} software from the fitted Gaussian peaks of three independent measurements and reported as the mode of distribution ± standard deviation.

Glutaraldehyde crosslinking

Glutaraldehyde crosslinking was performed by incubating 1 μM ClpC1, Sa ClpC, or Ec ClpB in buffer C (50 mM Hepes, 150 mM KCl, 20 mM $MgCl_2$, 5% [v/v] glycerol, and 2 mM DTT) in the absence or the presence of 2 mM ATPγS at 25 °C for 5 min. About 5 μM CymA or 0.5 μM ClpS were added as indicated. Crosslinking was started by adding glutaraldehyde (Sigma) to a final concentration of 0.1%. Aliquots were taken at indicated time points, and crosslinking was quenched by adding Tris (pH 7.5) to a final concentration of 50 mM. Samples were subjected to SDS-PAGE, and gels were stained with SYPRO Ruby Protein Gel Stain.

ATPase assay

The ATPase activity of ClpC1 was determined using coupled reactions of pyruvate kinase (PK) and lactate dehydrogenase (LDH) in the presence of phosphoenolpyruvate (PEP) and NADH. Briefly, PK regenerates ADP into ATP under conversion of PEP to pyruvate. Pyruvate is then reduced to lactate by LDH with NADH as electron donor. The consumption of NADH can be followed by measuring the absorbance decrease at 340 nm. The reactions were started with the addition of ATP followed by a 10-min incubation to allow for the assembly of ClpC1. Measurements were carried out at 30 °C in buffer D (50 mM Hepes [pH 7.5], 150 mM KCl, 20 mM $MgCl_2$, 1 mM DTT, and 10% [v/v] glycerol) in the presence of 5 mM ATP, 2 mM PEP (Sigma), 1 mM NADH (PanReak AppliChem), 6 U/ml PK (Roche), and 18 U/ml LDH (Sigma) using a BioTek Synergy 2 plate reader. Protein concentrations were as follows: 1 μM ClpC1, 2.3 μM Mtb ClpP1P2, 10 μM casein, and 5 μM CymA as indicated. Assays including Sa ClpP were done in buffer D at 30 °C in the presence of 2 mM ATP. Proteins were used at the following concentration: 1 μM ClpC1, 1.5 μM Sa ClpP, 10 μM casein, 1.5 μM ClpS. 2 μM FR-L-GFP, and 5 μM CymA as indicated. ATPase rates were calculated from the linear decrease of absorbance at 340 nm in at least three independent experiments, and standard deviations were calculated. All reactions included 1% (v/v) dimethyl sulfoxide (DMSO) to equal buffer conditions in the presence of CycA. The presence of DMSO did not affect ClpC1 activities.

Anisotropy measurements

Binding of ClpC1 to FITC-casein (100 nM) was monitored by fluorescence anisotropy measurements using a BMG Biotech CLARIOstar platereader. Samples were incubated in 50 mM Tris (pH 7.5), 25 mM KCl, 20 mM $MgCl_2$, and 5% (v/v) glycerol for 10 min at 30 °C in the presence of 2 mM ATP. About 10 μM CymA was added as indicated. Polarization of FITC-casein was determined in black 384-well plates (excitation: 482 nm; emission: 530 nm; and target mP: 35). A sample containing FITC-casein only served as reference. K_d values were determined using nonlinear regression curve fitting (Prism software; GraphPad Prism, Inc).

Degradation assays

All degradation assays were performed in buffer D (50 mM Hepes [pH 7.5], 150 mM KCl, 20 mM $MgCl_2$, 2 mM DTT, and 10% [v/v] glycerol) using 3 μM ClpC1, 4.5 μM ClpP1P2, 0.4 mM activator peptide (benzyloxycarbonyl-L-leucyl-L-leucinal; PeptaNova) in the presence of an ATP-regenerating system (6 U/ml PK and 5 mM PEP). Reactions included 10 μM CymA as indicated. Sa ClpP was used at 1.5 μM concentration. Substrates were used at the following concentrations: 0.5 μM GFP-SsrA, 0.5 μM FITC-casein (Sigma), 1 μM FR-L-GFP, and 5 μM VapB15. CymA was added to 10 μM final concentration. All reactions included 1% (v/v) DMSO to equal buffer conditions in the presence of CymA. The presence of DMSO did not affect ClpC activities. FITC-casein degradation was analyzed using a CLARIOstar plate reader, in black 96-well plates (Corning; nonbinding surface coated; flat bottom). The increase of FITC-casein fluorescence upon its degradation was monitored by using 483 and 520/530 nm as excitation and emission wavelengths, respectively. For data processing, the initial fluorescence intensities were set to 100. FITC-casein degradation rates were determined from the initial slopes of the fluorescence signal increase in at least three independent experiments, and standard deviations were calculated. For degradation of GFP-SsrA and FR-L-GFP, fluorescence was monitored in a 96-well plate (Corning; nonbinding surface coated, flat bottom) with a BioTek Synergy 2 Plate Reader using a 360/40 nm band-pass filter and 528/20 nm band-pass filter as excitation and emission wavelengths, respectively. Initial GFP fluorescence was set to 100. Degradation rates were determined from the initial slopes of fluorescence signal decrease in at least three independent experiments, and standard deviations were calculated.

Degradation of VapB15 was followed by SDS-PAGE. Reactions were incubated at 37 °C, and samples were taken at the indicated time points.

Negative-staining EM

ClpC1-WT and ClpC-F444S were in 20 mM Tris–HCl, pH 7.5, 20 mM KCl, 15 mM $MgCl_2$, and 1 mM DTT supplemented with 2 mM ATPγS. Proteins were applied to glow-discharged continuous carbon-coated grids (EM Sciences) and stained with 2% uranyl acetate. Micrograph movies were recorded on a Falcon 3 (Thermo Fisher Scientific) direct electron detector operated in linear mode at a magnification of 92,000× (pixel size = 1.54 Å/px; underfocus range = 0.5–1.2 μm) using a Talos Arctica microscope operated at 200 kV under low-dose conditions with a total dose of $20e^-$ divided into 20 frames. Movies were aligned using MotionCor2 (33), contrast transfer function was estimated with Gctf (34), particles were automatically picked with X-mipp (35), extracted on boxes of 400 pixels, and 2D classified with Relion 3.0 (MRC Laboratory of Molecular Biology) (36), all within the Scipion Box frame (37). Around 12,000 particles from 2D classes corresponding to the ClpC1-WT resting state were selected and used for 3D *ab initio* generation and refinement using Relion 3.0 (36). The final structure envelope at 25 Å resolution shows a spiral assembly, reminiscent of the Sa ClpC decamer. The Sa ClpC model was rigid body fitted, and density was assigned to the head-to-head locked MDs recognized (Fig. S1*D*). When displayed at high threshold, the skeleton of two ClpC1 hexamers or pentamers is seen (Fig. S1*D*).

In vivo *toxicity assay*

Ec XL1 cells harboring pUHE21-encoded *clpC1* alleles were grown in the absence of IPTG overnight at 30 °C. Cells in addition harbored the plasmids pDMI.1 or pDMI.1-Sa *clpP*. Absorbance values at 600 nm were adjusted to 1. Serial dilutions (10^{-1}–10^{-6}) were prepared, spotted on LB plates containing different IPTG concentrations, and incubated for 24 h at indicated temperatures. Spot tests were performed in two or more independent experiments each, and representative results are provided.

Data availability

All data are contained within the article.

Supporting information—This article contains supporting information (23–25, 38).

Author contributions—E. W.-B. and A. M. conceptualization; G. T., Y. F., P. K., D. L., M. C., and A.M. methodology; G. T., Y. F., P. K., D. L., M. C., and A. M. investigation; G. T., Y. F., P. K., D. L., M. C., E. W.-B., and A. M. formal analysis; A. M. writing–original draft; G. T., M. C., I.S., E. W.-B., and A.M. writing–review and editing; I. S., E. W.-B., and A. M. supervision; G. T., M. C., and A. M. visualization; E. W.-B. and A. M. funding acquisition.

Funding and additional information—This work was supported by a grant of the Deutsche Forschungsgemeinschaft (grant no.: MO970/4-3) to A.M. and by an ETH Zurich research grant (grant no.: ETH-40 16-1) to E.W.-B. P.K. was supported by the Heidelberg Biosciences International Graduate School.

Conflict of interest—The authors declare that they have no conflicts of interest with the contents of this article.

Abbreviations—The abbreviations used are: AAA, ATPase Associated with diverse cellular Activities; ADEP, acyldepsipeptide; Bs, *Bacillus subtilis*; CymA, CyclomarinA; DMSO, dimethyl sulfoxide; DWB, double Walker B variant; Ec, *Escherichia coli*; LDH, lactate dehydrogenase; MD, middle domain; Mtb, *Mycobacterium tuberculosis*; NTD, N-terminal domain; pArg, phosphoarginine; PEP, phosphoenolpyruvate; PK, pyruvate kinase; Sa, *Staphylococcus aureus*; SEC, size-exclusion chromatography; SEC–MALS, multi-angle light scattering measurements coupled to SEC run.

References

1. Sauer, R. T., and Baker, T. A. (2011) AAA+ proteases: ATP-fueled machines of protein destruction. *Annu. Rev. Biochem.* **80**, 587–612
2. Mahmoud, S. A., and Chien, P. (2018) Regulated proteolysis in bacteria. *Annu. Rev. Biochem.* **87**, 677–696
3. Olivares, A. O., Baker, T. A., and Sauer, R. T. (2016) Mechanistic insights into bacterial AAA+ proteases and protein-remodelling machines. *Nat. Rev. Microbiol.* **14**, 33–44
4. Gates, S. N., and Martin, A. (2020) Stairway to translocation: AAA+ motor structures reveal the mechanisms of ATP-dependent substrate translocation. *Protein Sci.* **29**, 407–419

5. Trentini, D. B., Suskiewicz, M. J., Heuck, A., Kurzbauer, R., Deszcz, L., Mechtler, K., *et al.* (2016) Arginine phosphorylation marks proteins for degradation by a Clp protease. *Nature* **539**, 48–53
6. Erbse, A., Schmidt, R., Bornemann, T., Schneider-Mergener, J., Mogk, A., Zahn, R., *et al.* (2006) ClpS is an essential component of the N-end rule pathway in Escherichia coli. *Nature* **439**, 753–756
7. Ziemski, M., Leodolter, J., Taylor, G., Kerschenmeyer, A., and Weber-Ban, E. (2021) Genome-wide interaction screen for Mycobacterium tuberculosis ClpCP protease reveals toxin-antitoxin systems as a major substrate class. *FEBS J.* **288**, 111–126
8. Schlothauer, T., Mogk, A., Dougan, D. A., Bukau, B., and Turgay, K. (2003) MecA, an adaptor protein necessary for ClpC chaperone activity. *Proc. Natl. Acad. Sci. U. S. A.* **100**, 2306–2311
9. Carroni, M., Franke, K. B., Maurer, M., Jager, J., Hantke, I., Gloge, F., *et al.* (2017) Regulatory coiled-coil domains promote head-to-head assemblies of AAA+ chaperones essential for tunable activity control. *Elife* **6**, e30120
10. Kirstein, J., Schlothauer, T., Dougan, D. A., Lilie, H., Tischendorf, G., Mogk, A., *et al.* (2006) Adaptor protein controlled oligomerization activates the AAA+ protein ClpC. *EMBO J.* **25**, 1481–1491
11. Wang, F., Mei, Z., Qi, Y., Yan, C., Hu, Q., Wang, J., *et al.* (2011) Structure and mechanism of the hexameric MecA-ClpC molecular machine. *Nature* **471**, 331–335
12. Bhandari, V., Wong, K. S., Zhou, J. L., Mabanglo, M. F., Batey, R. A., and Houry, W. A. (2018) The role of ClpP protease in bacterial pathogenesis and human diseases. *ACS Chem. Biol.* **13**, 1413–1425
13. Akopian, T., Kandror, O., Raju, R. M., Unnikrishnan, M., Rubin, E. J., and Goldberg, A. L. (2012) The active ClpP protease from M. tuberculosis is a complex composed of a heptameric ClpP1 and a ClpP2 ring. *EMBO J.* **31**, 1529–1541
14. Famulla, K., Sass, P., Malik, I., Akopian, T., Kandror, O., Alber, M., *et al.* (2016) Acyldepsipeptide antibiotics kill mycobacteria by preventing the physiological functions of the ClpP1P2 protease. *Mol. Microbiol.* **101**, 194–209
15. Brotz-Oesterhelt, H., and Vorbach, A. (2021) Reprogramming of the caseinolytic protease by ADEP antibiotics: molecular mechanism, cellular consequences, therapeutic potential. *Front. Mol. Biosci.* **8**, 690902
16. Lee, H., and Suh, J. W. (2016) Anti-tuberculosis lead molecules from natural products targeting Mycobacterium tuberculosis ClpC1. *J. Ind. Microbiol. Biotechnol.* **43**, 205–212
17. Brotz-Oesterhelt, H., Beyer, D., Kroll, H. P., Endermann, R., Ladel, C., Schroeder, W., *et al.* (2005) Dysregulation of bacterial proteolytic machinery by a new class of antibiotics. *Nat. Med.* **11**, 1082–1087
18. Kirstein, J., Hoffmann, A., Lilie, H., Schmidt, R., Rübsamen-Waigmann, H., Brötz-Oesterhelt, H., *et al.* (2009) The antibiotic ADEP reprogrammes ClpP, switching it from a regulated to an uncontrolled protease. *EMBO Mol. Med.* **1**, 37–49
19. Schmitt, E. K., Riwanto, M., Sambandamurthy, V., Roggo, S., Miault, C., Zwingelstein, C., *et al.* (2011) The natural product cyclomarin kills Mycobacterium tuberculosis by targeting the ClpC1 subunit of the caseinolytic protease. *Angew. Chem. Int. Ed. Engl.* **50**, 5889–5891
20. Gavrish, E., Sit, C. S., Cao, S., Kandror, O., Spoering, A., Peoples, A., *et al.* (2014) Lassomycin, a ribosomally synthesized cyclic peptide, kills mycobacterium tuberculosis by targeting the ATP-dependent protease ClpC1P1P2. *Chem. Biol.* **21**, 509–518
21. Gao, W., Kim, J. Y., Anderson, J. R., Akopian, T., Hong, S., Jin, Y. Y., *et al.* (2015) The cyclic peptide ecumicin targeting ClpC1 is active against Mycobacterium tuberculosis *in vivo*. *Antimicrob. Agents Chemother.* **59**, 880–889
22. Choules, M. P., Wolf, N. M., Lee, H., Anderson, J. R., Grzelak, E. M., Wang, Y., *et al.* (2019) Rufomycin targets ClpC1 proteolysis in Mycobacterium tuberculosis and M. Abscessus. *Antimicrob. Agents Chemother.* **63**, e02204-18
23. Vasudevan, D., Rao, S. P., and Noble, C. G. (2013) Structural basis of mycobacterial inhibition by cyclomarin A. *J. Biol. Chem.* **288**, 30883–30891
24. Wolf, N. M., Lee, H., Choules, M. P., Pauli, G. F., Phansalkar, R., Anderson, J. R., *et al.* (2019) High-resolution structure of ClpC1-rufomycin and ligand binding studies provide a framework to design and optimize anti-tuberculosis leads. *ACS Infect. Dis.* **5**, 829–840
25. Wolf, N. M., Lee, H., Zagal, D., Nam, J. W., Oh, D. C., Lee, H., *et al.* (2020) Structure of the N-terminal domain of ClpC1 in complex with the antituberculosis natural product ecumicin reveals unique binding interactions. *Acta Crystallogr. D Struct. Biol.* **76**, 458–471
26. Maurer, M., Linder, D., Franke, K. B., Jager, J., Taylor, G., Gloge, F., *et al.* (2019) Toxic activation of an AAA+ protease by the antibacterial drug cyclomarin A. *Cell Chem Biol.* **26**, 1169–1179.e4
27. Leodolter, J., Warweg, J., and Weber-Ban, E. (2015) The Mycobacterium tuberculosis ClpP1P2 protease interacts asymmetrically with its ATPase partners ClpX and ClpC1. *PLoS One* **10**, e0125345
28. Schmitz, K. R., and Sauer, R. T. (2014) Substrate delivery by the AAA+ ClpX and ClpC1 unfoldases activates the mycobacterial ClpP1P2 peptidase. *Mol. Microbiol.* **93**, 617–628
29. Deville, C., Franke, K., Mogk, A., Bukau, B., and Saibil, H. R. (2019) Two-step activation mechanism of the ClpB disaggregase for sequential substrate threading by the main ATPase motor. *Cell Rep.* **27**, 3433–3446.e4
30. Kotamarthi, H. C., Sauer, R. T., and Baker, T. A. (2020) The non-dominant AAA+ ring in the ClpAP protease functions as an anti-stalling motor to accelerate protein unfolding and translocation. *Cell Rep.* **30**, 2644–2654.e3
31. Marsee, J. D., Ridings, A., Yu, T., and Miller, J. M. (2018) Mycobacterium tuberculosis ClpC1 N-terminal domain is dispensable for adaptor protein-dependent allosteric regulation. *Int. J. Mol. Sci.* **19**
32. Morreale, F. E., Kleine, S., Leodolter, J., Ovchinnikov, S., Kley, J., Kurzbauer, R., *et al.* (2021) BacPROTACs mediate targeted protein degradation in bacteria. *Cell* **185**, 2338–2353.e18
33. Zheng, S. Q., Palovcak, E., Armache, J. P., Verba, K. A., Cheng, Y., and Agard, D. A. (2017) MotionCor2: anisotropic correction of beam-induced motion for improved cryo-electron microscopy. *Nat. Methods* **14**, 331–332
34. Zhang, K. (2016) Gctf: Real-time CTF determination and correction. *J. Struct. Biol.* **193**, 1–12
35. Abrishami, V., Zaldivar-Peraza, A., de la Rosa-Trevin, J. M., Vargas, J., Oton, J., Marabini, R., *et al.* (2013) A pattern matching approach to the automatic selection of particles from low-contrast electron micrographs. *Bioinformatics* **29**, 2460–2468
36. Zivanov, J., Nakane, T., Forsberg, B. O., Kimanius, D., Hagen, W. J., Lindahl, E., *et al.* (2018) New tools for automated high-resolution cryo-EM structure determination in RELION-3. *Elife* **7**, e42166
37. de la Rosa-Trevin, J. M., Quintana, A., Del Cano, L., Zaldivar, A., Foche, I., Gutierrez, J., *et al.* (2016) Scipion: a software framework toward integration, reproducibility and validation in 3D electron microscopy. *J. Struct. Biol.* **195**, 93–99
38. Zeth, K., Ravelli, R. B., Paal, K., Cusack, S., Bukau, B., and Dougan, D. A. (2002) Structural analysis of the adaptor protein ClpS in complex with the N-terminal domain of ClpA. *Nat. Struct. Biol.* **9**, 906–911